Correlated Magnetic Noise in the Advanced LIGO Detector

Sylvia Biscoveanu and Eric Thrane
School of Physics and Astronomy
Monash University

August 10, 2015

Abstract

A stochastic gravitational wave background is expected to arise as the result of many overlapping, individually indistinguishable sources. Such a background is measured by correlating the strain signal in two detectors like those part of the Laser Interferometer Gravitational Wave Observatory (LIGO). The two detectors must be sufficiently far apart to minimize common noise sources, which create correlated noise that doesn't decrease with increased integration time. One possible source of correlated noise is Schumann resonances–global magnetic fields produced by lightning strikes that excite the Earth-Ionosphere cavity. After a series of updates designed to improve detector sensitivity, the Advanced LIGO (aLIGO) instrument will begin its first science run in the Fall of 2015. In this paper, we analyze the magnetic contribution to correlated noise and present an updated noise budget for the data from the latest engineering run in preparation for aLIGO's first science run.

1 Introduction

1.1 The Stochastic Background

A random gravitational wave background is predicted as a result of many overlapping, individually indistinguishable sources that are both astrophysical and cosmological in nature. Such sources include coalescing binaries, core collapse supernovae, inflation, phase transitions, and cosmic strings, among others [1]. Detection of this gravitational wave signature would offer insight into the state of the universe in the moments immediately following the Big Bang.

When conducting searches for the stochastic background, one typically seeks to measure the ratio of the energy contribution due to gravitational waves to the critical energy density needed to close the universe,

$$\Omega_{gw} = \frac{1}{\rho_c}\frac{d\rho_{gw}}{d\ln f}. \tag{1}$$

The critical density is defined as

$$\rho_c = \frac{3c^2 H_0^2}{8\pi G}, \tag{2}$$

and H_0 is the Hubble expansion rate [1]. This quantity describes the spectrum of the stochastic background as a function of frequency and is often modeled as a power law,

$$\Omega_{gw} = \Omega_\alpha f^\alpha, \tag{3}$$

where $\alpha = 2/3$ for astrophysical backgrounds and $\alpha = 0$ for cosmological sources [2]. The current best upper limit on the stochastic gravitational wave background energy density from the ground-based LIGO and VIRGO detectors is $\Omega_{gw} < 5.6 \times 10^{-6}$ [3].

Certain statistical assumptions must be made to give a more robust description of the stochastic background than that provided by the spectrum alone. We assume that such a background is stationary, isotropic, unpolarized, and Gaussian. For a signal to be stationary, it must depend only on the differences between times and not on the absolute times themselves. Because the age of the universe is at least 20 orders of magnitude larger than the expected period of gravitational waves that could be detected with ground–based interferometers, no time dependence is anticipated [1].

If the stochastic background is analogous to the Cosmic Microwave Background, it is justified to assume that it would be highly isotropic. However, the directional dependence of the background will ultimately depend on its sources, so this assumption may be false. For example, a stochastic background dominated by coalescing binaries in one area of the sky will be highly anisotropic, while one resulting largely from cosmological sources will show no directional dependence.

An unpolarized background is composed equally of waves with plus and cross polarizations. The final assumption is proven by the Central Limit Theorem, which states that any random process created by the superposition of independent random variables will be Gaussian [5]. As long as the stochastic background is a result of many overlapping and independent gravitational wave signals, it's statistical properties will be entirely determined by the first and second moments of the strain recorded in a detector.

1.2 Advanced LIGO

In order to detect such a signal, the strain data from two detectors must be cross–correlated. The Laser Interferometer Gravitational Wave Observatory (LIGO) is a pair of ground based interferometers located in Hanford, Washington, and Livingston, Louisiana. Each detector consists of a Michelson Interferometer with 4 km long arms, with a Fabry–Pérot cavity in each arm. Laser light is sent to a beam splitter, which in turn redirects the beam to travel down the two arms. Upon reaching the end optics, the light is reflected and recombined at the beam splitter and sent to a photodetector. The effect of a gravitational

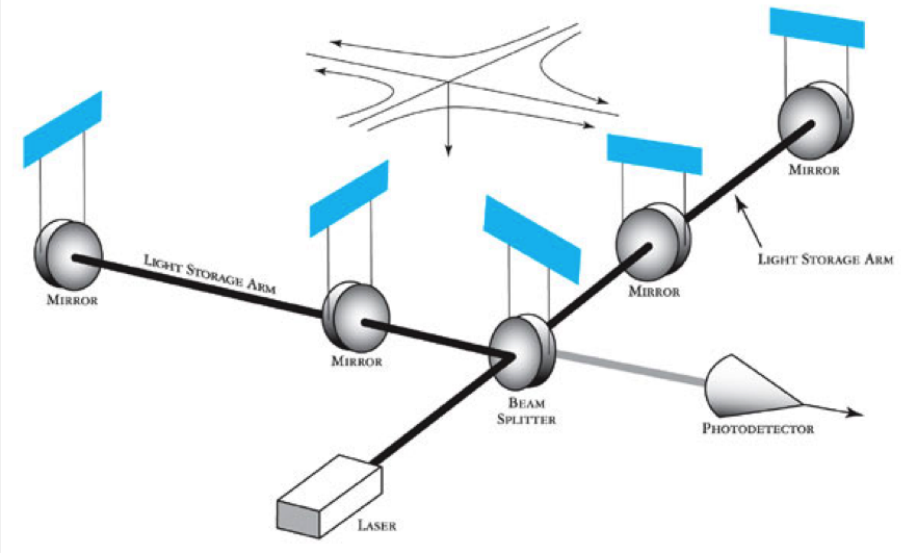

Figure 1: Schematic of a Michelson Interferometer from [4] like the one used in the two LIGO observatories. Laser light incident on the beam splitter is sent down the two arms and reflected back by the end test mass. In the presence of a gravitational wave, the arm length will be compressed in one direction and extended in the other, leading to a phase shift observable as an interference pattern in the recombined light received by the photodetector.

wave would be to compress the arm length in one direction while stretching it in the perpendicular direction. This would result in a phase shift between the two light beams, which would produce an interference pattern that would be recorded by the photodetector upon recombination [6].

After a series of updates to the Initial LIGO instrument, the Advanced LIGO (aLIGO) detector will begin its first science run in the Fall of 2015. The laser power was increased from 10 W to 100 W, with a corresponding increase in both the diameter and the mass of the end mirrors. Initial LIGO used 25 cm, 11 kg fused silica masses, while those used in aLIGO are 34 cm with a mass of 40 kg. The diameter increase will counteract thermal noise and the increase in mass minimizes the effects of shot noise. The suspension system has also been upgraded to a four–pendulum setup, with fused silica fibers replacing the previously used steel wires. This upgrade to the seismic isolation system has extended the lower limit of the frequency band from 40 Hz down to 10 Hz [7].

The combined effect of the system upgrades will be to improve the sensitivity across the entire frequency spectrum by at least a factor of 10 and to deepen the field of view of the detector. For example, binary systems made up of $1.4M_{\odot}$ inspiraling neutron stars will be detectable at distances 15 times greater than with initial LIGO [7]. The uncertainty in the energy density measurement

calculated with two weeks of aLIGO engineering run data already shows a factor of 8 improvement over the last initial LIGO science run [8].

1.3 Noise Sources

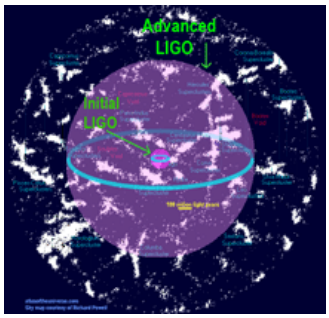

Figure 2: Image from [7] showing that the observable volume of space of aLIGO is 1000 times that of initial LIGO.

Sensitivity limitations arise from external forces on the test masses and a limited ability to detect the response to gravitational wave strain. The mirrors are suspended as pendulums and modeled as free falling masses to minimize the latter, while the former is corrected through the use of a servomechanism which induces artificial magnetic fields via an electromagnetic coil [9]. Small magnets attached to the optics respond to these fields, effectively keeping them in place. The arms are kept under tight vacuum to minimize light scattering from residual gas molecules. Thermal noise dominates the LIGO frequency band, while other noise sources include seismic noise, shot noise–the effect of the momentum transfer of the individual photons hitting the test mass–and local anthropogenic noise mostly due to electronics [5].

The detectors used for the stochastic measurement must be sufficiently far apart to minimize common noise sources, since a key assumption in the stochastic search is that the noise observed is uncorrelated [1]. While a large geographic distance between the two interferometers will successfully eliminate common anthropogenic noise, global magnetic fields called Schumann resonances do create correlated noise in the detectors. Schumann resonances arise from lightning strikes that create standing waves in the cavity formed by the surface of the Earth and the lower edge of the ionosphere. A background of about 100 lightning strikes/s generates a current of 20-30 kA, which corresponds to a magnetic field on Earth's surface on the order of pT. These resonances create a harmonic series with the fundamental at 8 Hz and primary and secondary overtones at 14 and 20 Hz, respectively. Such magnetic fields create correlated noise by coupling to the magnets used as part of the detector's servomechanism. Because the magnetic fields generated by Schumann resonances are coherent on length scales of 1000 km, magnetic contamination will appear in both detectors [10].

This analysis will provide an update on the status of correlated magnetic noise in the aLIGO detector. The data used is from the latest aLIGO engineering run, which occurred between June 3rd and June 14th, 2015. An updated noise budget and signal to noise ratio calculation will be presented, along with a discussion on incorporating these measurements into a real-time web-based monitoring tool called Stochmon (short for Stochastic Monitor), which will be used to track the quality of stochastic background data during the aLIGO science run.

2 Formalism

The total strain, s is each detector can be written as:

$$\tilde{s}(f) = \tilde{h}(f) + \tilde{n}(f) + r(f)\tilde{m}(f), \tag{4}$$

where h is the astrophysical contribution, n is local uncorrelated noise, m is the correlated magnetic noise, and r is the coupling function used to convert the magnetic signal to strain. We also define a set of power spectra to characterize the different strain contributions.

$$\begin{aligned} H(f) &\equiv k\langle \tilde{h}_1^*(f)\tilde{h}_2(f)\rangle \\ M(f) &\equiv k\langle \tilde{m}^*(f)\tilde{m}(f)\rangle \\ P_{12}(f) &\equiv k\langle \tilde{s}_1^*(f)\tilde{s}_2(f)\rangle \\ P_I(f) &\equiv k\langle \mid \tilde{s}_I(f) \mid^2\rangle \\ H_M(f) &\equiv \mathrm{Re}[r(f)^2 M(f)], \end{aligned} \tag{5}$$

where k is the Fourier normalization constant. H is the astrophysical strain cross-power spectrum, M is the correlated magnetic noise power-spectrum, P_{12} is the total cross power spectrum, P_I is the auto power spectrum for detector I, and H_M is the correlated strain noise power spectrum. The uncertainty, σ associated with H is given by:

$$\sigma(f) = \left[\frac{1}{2N_{seg}}\overline{P_1 P_2}\right]^{1/2}, \tag{6}$$

where N_{seg} is the number of time chunks included in the calculation. To convert from power spectrum to energy density, the following relationship is used:

$$\Omega_{gw}(f) = \frac{2\pi^2}{3H_0^2} f^3 \frac{5}{|\gamma(f)|} S(f), \tag{7}$$

for any power spectrum, S. In the case of the energy density due to magnetic contamination, Ω_M, H_M is used. σ can also be converted to σ_{gw} by using it in place of S in the above equation [11]. γ is the overlap reduction function, which is a function of the geometrical properties of the two detectors in question.

For any two coincident and coaligned detectors, γ is normalized to 1, but a separation between the detectors or lack of perfectly parallel arm alignment will result in a decrease in sensitivity. These two factors imply that there is only partial overlap between the gravitational strains recorded in the two detectors, an effect which is quantized by the overlap reduction function [1]. For a detailed calculation of γ for the Hanford-Livingston detector pair given in Figure 3, see [2].

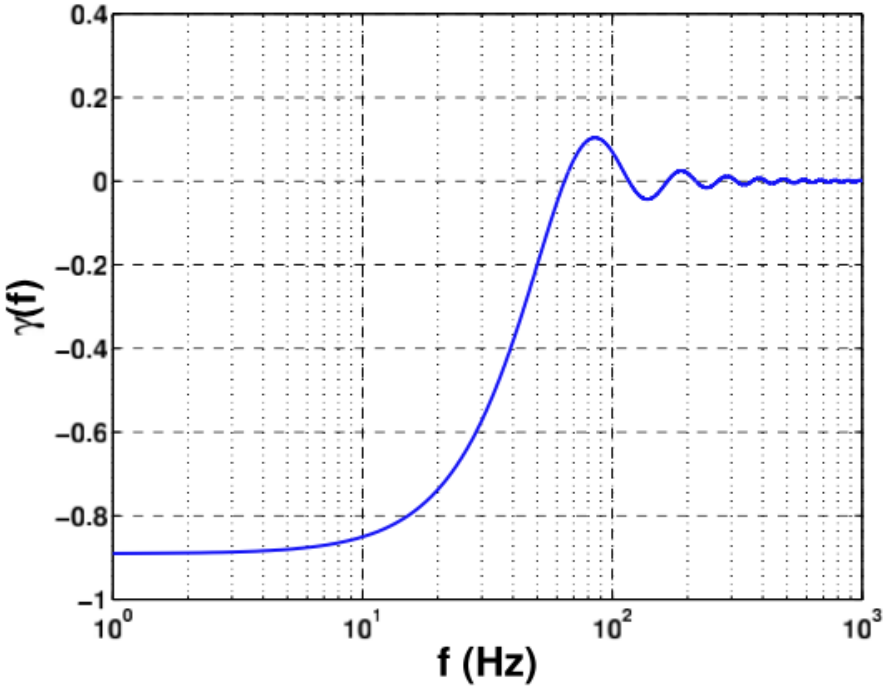

Figure 3: Overlap reduction function for the Hanford-Livingston detector pair from [2].

In order to calculate the signal to noise ratio (SNR), we define the broadband estimators:

$$\Omega_M(\alpha) = \frac{\int df \Omega_M(f) \sigma_{gw}^{-2}(f)}{\int \sigma_{gw}^{-2}(f)}, \tag{8}$$

$$\sigma_{gw}(\alpha) = \left[\int df \sigma^{-2}(f) \right]^{-1/2}. \tag{9}$$

In terms of these two estimators, the signal to noise ratio then becomes:

$$\mathrm{SNR} = \frac{\langle \Omega_M(\alpha) \rangle}{\sigma_{gw}(\alpha)}. \tag{10}$$

Another way to determine the level of correlation between the signals in two detectors is to calculate the coherence:

$$\mathrm{coh}(f) \equiv \frac{|\overline{\tilde{s}_1^*(f)\tilde{s}_2(f)}|^2}{|\tilde{s}_1(f)|^2 |\tilde{s}_2(f)|^2}, \tag{11}$$

or in terms of power spectra,

$$\mathrm{coh}(f) \equiv \frac{|\overline{P_{12}(f)}|^2}{\overline{P_1(f)}\,\overline{P_2(f)}}, \tag{12}$$

where the overline denotes time averaging over N_{seg}. For independent, Gaussian, and stationary strain signals, $\langle \mathrm{coh}(f) \rangle = 1/N_{seg}$ [10]. Excess coherence is indicative of correlation in the signal, while minimums in the coherence spectra may reveal nonstationarity effects.

3 Results

3.1 Coherence

Coherence was calculated both for the detector's strain channels and magnetometer channels. In the strain channel coherence spectrum (Figure 4), no broadband features are apparent, but a narrowband peak is observed at 64 Hz. This is due to the overlapping power grid oscillations at both sites. Dips in the coherence spectrum like the one observed at 500 Hz are likely due to nonstationarity glitches–periods of increased (or decreased) noise at one detector due to local environmental or anthropogenic effects. Such noisy or quiet periods are time dependent, and manifest themselves as dips in the spectrum.

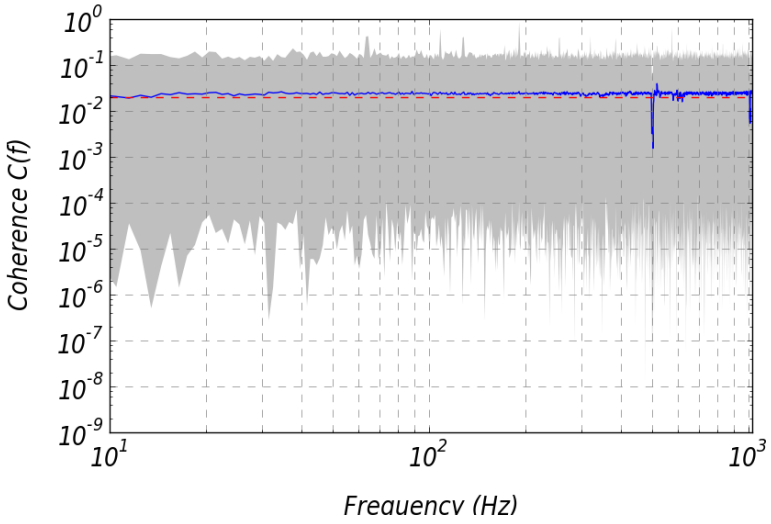

Figure 4: Coherence spectrum for the Hanford-Livingston strain channels using data from the entire engineering run sampled at 1 mHz. The blue curve plots the mean for each 1 Hz bin while the gray area spans from the max to the min.

If the data analyzed spans a long enough period of time–usually on the order of a couple months–broadband peaks due to Schumann resonances should be observed in the coherence spectra for the magnetometer channels [10]. Both detectors are equipped with several of these instruments as part of the Physical and Environmental Monitoring (PEM) system, and those used in this analysis

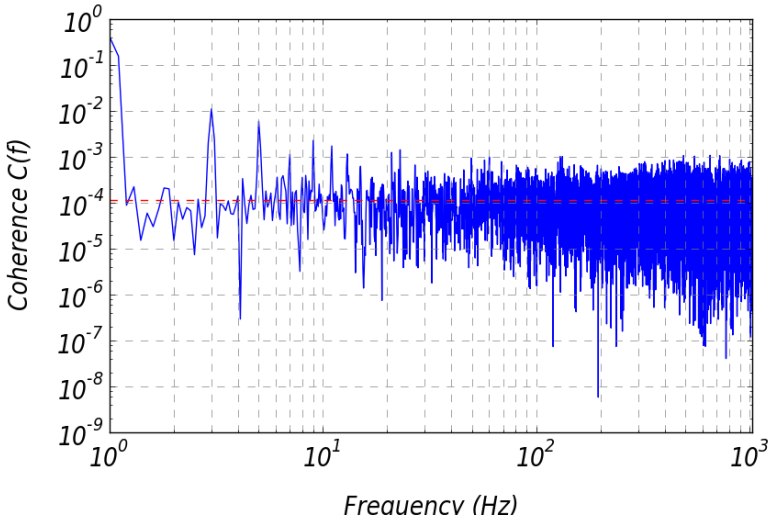

Figure 5: Coherence spectrum for the Hanford-Livingston PEM-LVEA magnetometer channels using data coincident with the engineering run sampled at 10 mHz.

are from the Laser and Vacuum Equipment Area (LVEA) at the corner station of each observatory [12]. Just under two weeks of data was analyzed, selected to coincide with the strain channel data from the engineering run. Broadband peaks are not observed in Figure 5, but the narrowband peaks observed at 3 Hz and 5 Hz are likely due to electronic noise.

3.2 Coupling function

The coupling function, r, used to convert from magnetic signal to strain, can have a huge effect on the overall SNR calculated. This function is determined by measuring the response of the test masses to artificial fields induced near the detector using Helmholtz injection coils. Figure 6 gives the length coupling function used in initial predictions of magnetic contamination in aLIGO from [13]. For the most conservative measurement, r is given by the maximum coupling value at each frequency, and then modeled as a power law. This approximation is valid within a factor of ≈ 2 [11].

Measurements of the coupling function were repeated again in June 2015. The updated plot from [14] is shown in Figure 7. A reduction of at least one order of magnitude is observed, although the source of this improvement is unknown. This leads to a significant reduction in the magnetic SNR, as will be described in the next section. For this analysis, the coupling function is parametrized as a piecewise power law, as demonstrated in Figure 8.

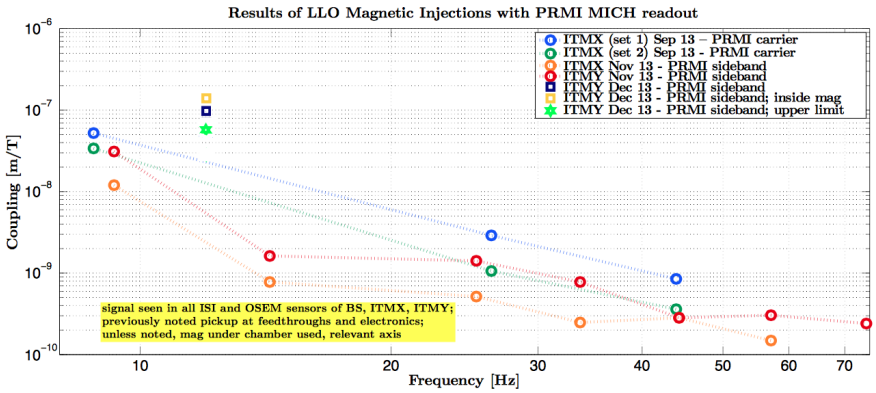

Figure 6: Coupling function from [13] for the length degree of freedom from March 2014. The different symbols represent different test masses.

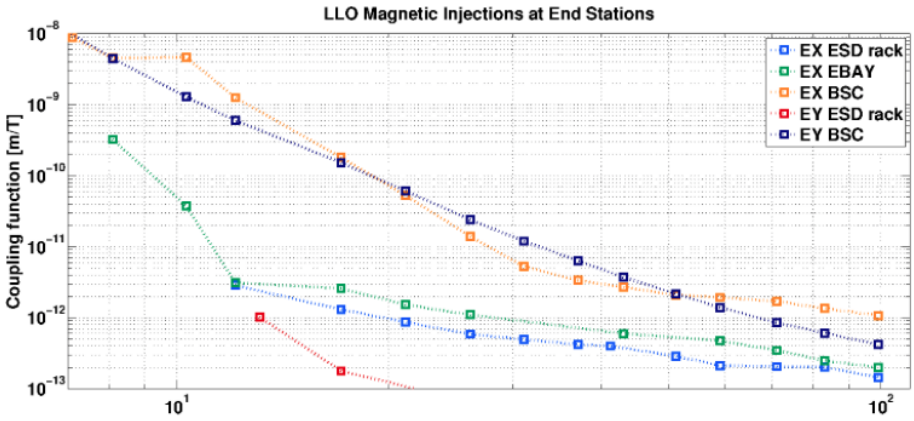

Figure 7: Coupling function from [14] for combined length and angular degrees of freedom from June 2015.

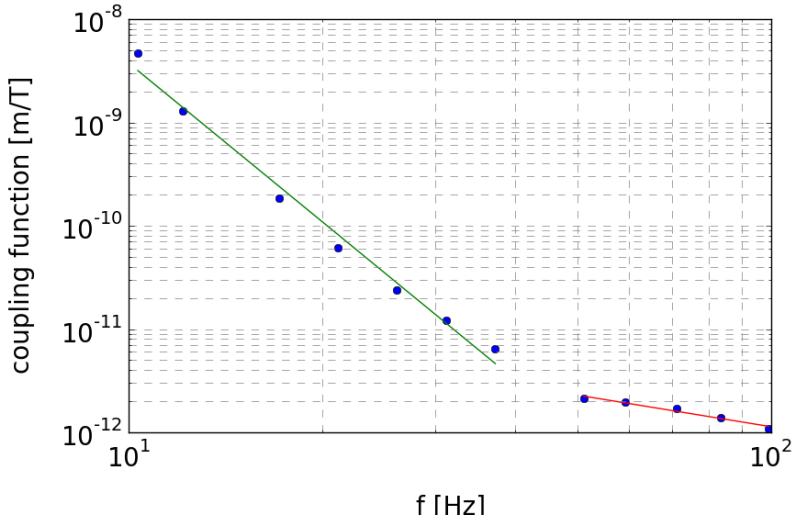

Figure 8: Power law parametrization for the maximum coupling values for each frequency shown in Figure 7. For the points up to 41.08 Hz, the spectral index is -5.10, and for higher frequencies the shallower index of -1.02 is used.

3.3 Power Law Integrated Curves

Before presenting the correlated noise budget, we explain the construction of the power law integrated curves used to represent the broadband sensitivity of the detector. $\Omega_{\rm eff}$ is calculated using Equation 7 for power spectrum P_{12} given in Equation 5. As in Equation 3, we model Ω_{gw} as a power law, and Ω_α is given for each spectral index by:

$$\Omega_\alpha = \rho \left[\int_{f_{min}}^{f_{max}} df \, \frac{f^{2\alpha}}{\Omega_{\rm eff}^2(f)} \right]^{-1/2} \tag{13}$$

where ρ is the integrated signal to noise ratio–in this case set to $\rho = 1$ [2]. We then plot Ω_{gw} as given by Equation 3 for a set of spectral indices, $-8 \leq \alpha \leq 8$, with $\delta\alpha = 1/3$. The power law integrated curve is the outline formed by these individual curves for Ω_α shown in Figure 9. Formally, it is given by:

$$\Omega_{\rm PI} = \max \left[\Omega_\alpha f^\alpha \right]. \tag{14}$$

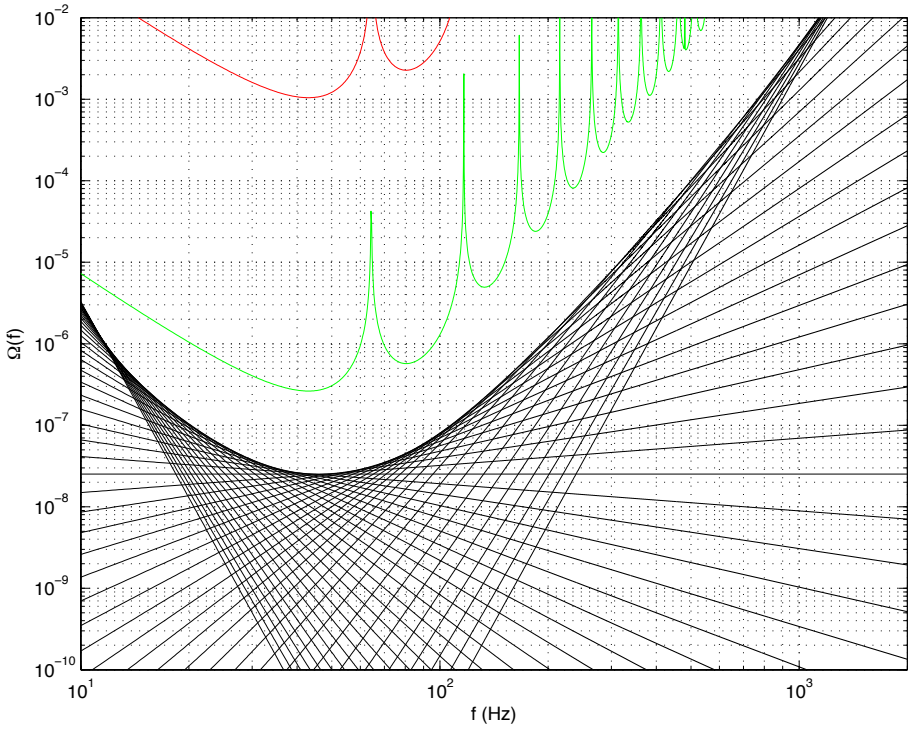

Figure 9: Ω_{gw} sensitivity curves for the predicted sensitivity that will be reached during aLIGO's first science run in the Fall. The red shows Ω_{eff}, while the green plots $\Omega_{\text{eff}}/\sqrt{2T\delta f}$. This is the optimal combination of one year's worth of data with a typical bin size of 0.25 Hz., and the peaks are due to the zeroes of the overlap reduction function [2]. The black lines correspond to Ω_{gw} for each spectral index. Their outline forms Ω_{PI}.

3.4 Noise Budget

The correlated noise budget taken from [11] calculated with the March 2014 coupling function is given in Figure 10. Ω_M is calculated for coupling to both the length (red) and angular degrees of freedom. The angular coupling is dependent on the beam offset from the end mirror's axis of rotation, so predictions are made for 1 mm (purple) and 3 mm (turquoise) offsets. The sensitivity shown in green in this figure is the predicted maximum sensitivity that will be reached during aLIGO's five year run. The power law integrated curve is given in black, with dashed black representing the energy density for a flat spectrum ($\alpha = 0$). Correlated magnetic noise is significant if Ω_M falls above the power law integrated curve, and in this case, SNR $\lesssim 330 - 470$ [11].

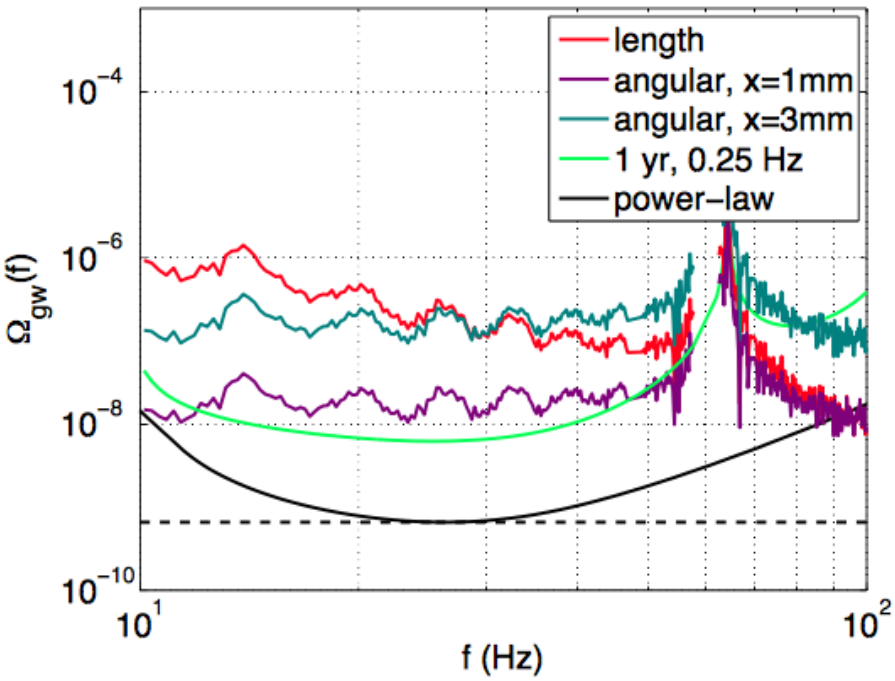

Figure 10: Correlated noise budget from [11] calculated using the coupling function from March 2014. Red shows magnetic contamination due to coupling to the length degree of freedom, while purple and turquoise are for coupling to the angular degree of freedom with a beam offset of 1 mm and 3 mm, respectively. Green shows the narrowband sensitivity for one year of data and 0.25 Hz bins, assuming that the detector is running at the maximum sensitivity expected for aLIGO. Black is the power law integrated curve, and dashed black is the energy density for a flat spectrum [11].

Figure 11 shows the effect of an order of magnitude improvement in the coupling function as discussed in Section 3.2. Using the coupling function measured in June 2015, magnetic contamination is combined for coupling to all degrees of freedom (red), and falls below the power law integrated curve with the exception of low frequencies. Ω_M is reduced by at least two orders of magnitude, but will still need to be accounted for once design sensitivity is reached.

We reproduce the noise budget using data from the latest engineering run in Figure 12. The dark blue curve represents narrowband detector sensitivity, while the broadband sensitivity is given by the black power law integrated curve. The light blue curve shows the magnetic contamination, Ω_M. The peaks in both of the blue curves are due to the zeroes of the overlap reduction function. With the exception of these peaks, Ω_M falls exclusively below the black power law integrated curve, which indicates that this magnetic signal will not cause

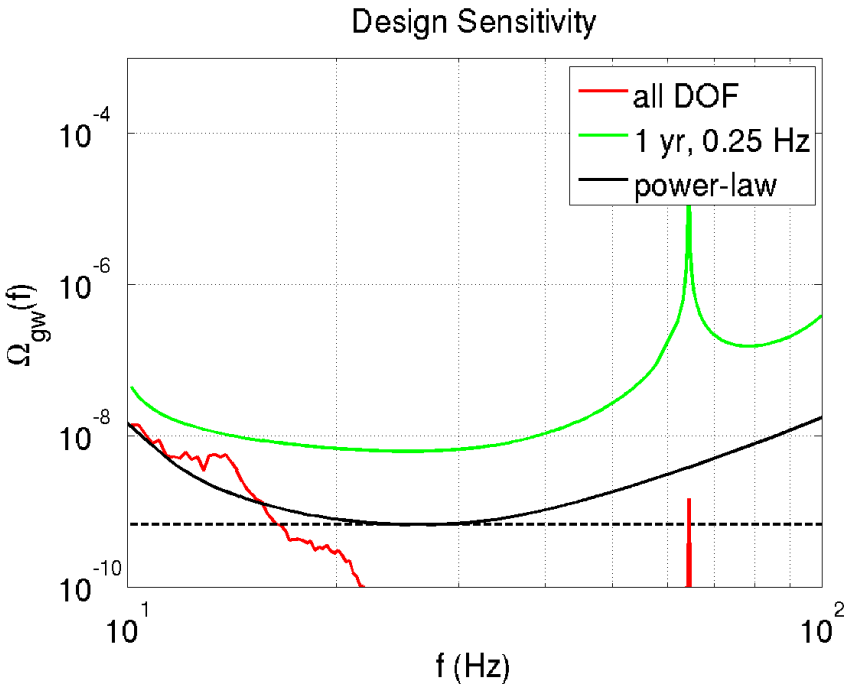

Figure 11: Correlated noise budget calculated using the coupling function from June 2015. Red is magnetic contamination due to coupling to all degrees of freedom, green is the narrowband sensitivity for one year of data with 0.25 Hz bins, and black is the power law integrated curve and corresponding energy density for a flat spectrum (dashed line). Magnetic contamination is reduced by at least two orders of magnitude compared to Figure 10.

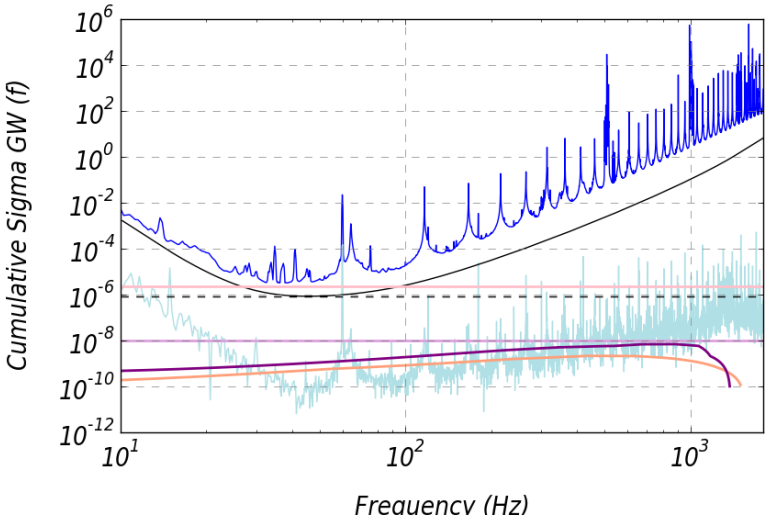

Figure 12: Correlated noise budget calculated using strain and magnetometer data from the latest engineering run and the coupling function from June 2015. Dark blue shows detector sensitivity while light blue represents magnetic contamination. Broadband sensitivity is given by the black power law integrated curve, while the dashed black gives the energy density assuming a flat spectrum. The orange curve gives the predicted background for binary neutron star systems with $M_c = 1.22M_\odot$ for a realistic local binary coalescence rate of $1.54\text{Mpc}^{-3}\text{Myr}^{-1}$ [15]. The dark purple gives the same estimate but for the binary black hole case for $M_c = 6.72M_\odot$ and a local semi-optimistic rate of $0.17\text{Mpc}^{-3}\text{Myr}^{-1}$ [16]. The pink and light purple curves taken from [3] give the predicted contribution due to the CMB and matter spectra and cosmic strings, respectively.

significant contamination. In fact, the SNR calculated using engineering run data assuming a flat spectrum is 0.001036. We also include several astrophysical and cosmological backgrounds for comparison to the detector sensitivity.

3.5 Sensitivity Prediction

In order to determine how the detector sensitivity improves with continued integration time, we calculate the sensitivity prediction for five years of integration assuming the sensitivity level reached during the latest engineering run is maintained. Figure 13 shows these predictions as well as the real time evolution of σ_{gw} during the engineering run alongside the astrophysical and cosmological backgrounds as a reference. The dark blue, red, and green give the sensitivity assuming the background is dominated by astrophysical sources ($\alpha = 2/3$) while the lighter colors are for a flat spectrum dominated by cosmological sources

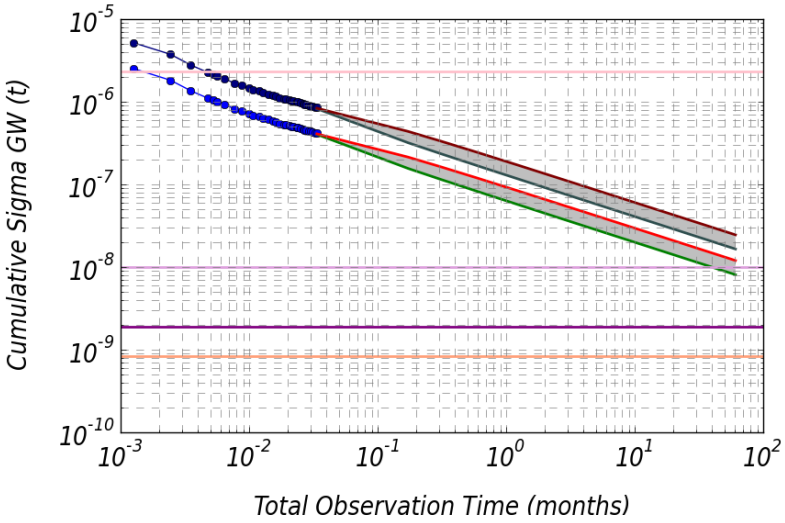

Figure 13: Sensitivity prediction for 5 years assuming the detector continues to run at the sensitivity reached during the engineering run. The blue points show the real time σ evolution during the run, while the red and green lines give the predictions assuming the detector runs at the mean and best sensitivity reached during the run, respectively. The darker colors correspond to a background dominated by astrophysical sources, while the lighter colors give the σ for a cosmologically dominated background. The orange, lilac, pink, and purple curves are the astrophysical and cosmological energy density predictions as explained in Figure 12.

($\alpha = 0$). σ_{gw} is calculated using Equation 9 in real time (blue points), and the predicted σ is given by:

$$\sigma_{gw} = \left[\sigma_{\rm tot}^2 + M\sigma_{\rm new}^2\right]^{-1/2} \tag{15}$$

where σ_{tot} is the sensitivity reached in the last hour of real data, M is the number of hours since the end of the engineering run, and $\sigma_{\rm new}$ is the assumed continued sensitivity of the detector. The predictions for two different assumed sensitivities are shown. The red lines give the prediction assuming that the detector continues to run at the mean hourly σ calculated for the entire engineering run, while the green is for the peak σ achieved during the run. The cosmological and astrophysical backgrounds are the same as in Figure 12, with Ω_{gw} for the BBH and BNS cases calculated at a reference frequency of 100Hz.

4 Concluding Remarks

We present the updated correlated noise budget calculated using data from the latest engineering run in preparation for aLIGO's first science run in the Fall of 2015. The effects of an order of magnitude improvement in the magnetic coupling function are explored, and we observe that the magnetic signal to noise ratio decreases from SNR $\lesssim 330-470$ to SNR $= 0.001036$. Despite this substantial improvement, correlated magnetic noise will continue to be significant at low frequencies in the advanced LIGO detector. We also explore the long term detector sensitivity predictions, and conclude that if the detector continues to run at the sensitivity reached during the engineering run, the astrophysical backgrounds due to BSN and BBH will not be detected. However, by the time design sensitivity is reached in 2019, detection of gravitational waves from these sources is expected [7].

The results presented in the previous section are useful tools for detector characterization. A new initiative for the aLIGO science run is to include these plots, among others, in a real-time, web-based monitoring tool of the quality of the stochastic background data. This tool is called Stochmon, short for Stochastic Monitor, and was created by Tom Callister–a graduate student at Caltech–under the supervision of Dr. Eric Thrane. We have added the plots of magnetometer coherence, the correlated noise budget, and the sensitivity predictions to the Stochmon webpage for a more robust description of the quality of data. During the aLIGO run, Stochmon will update with new data on an hourly basis, and this will help detect and fix problems as they occur instead of after the data run as was done during initial LIGO. Stochmon will prove to be an important resource for detector monitoring and tracking data quality.

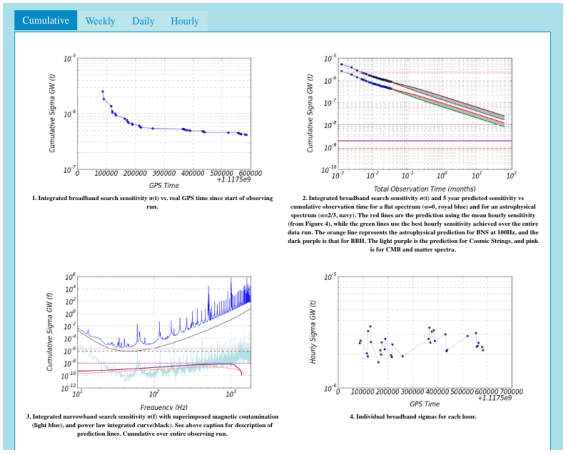

Figure 14: Screenshot of the Stochmon webpage. Results using cumulative, weekly, daily, and hourly data are available on separate tabs. Plots of hourly and integrated σ are included, as well as strain and magnetometer channel coherence, the sensitivity predictions, and the updated correlated noise budget [8].

Special thanks to the National Science Foundation for sponsoring this International REU program. Thank you also to Dr. Bernard Whiting, Dr. Guido Mueller, and Kristin Nichola at the University of Florida for giving me the opportunity to participate in this program and for organizing my stay and collaboration with Monash University. Thank you to my supervisor, Dr. Eric Thrane for his incredible patience and support, and to Tom at Caltech for being so willing to help with Stochmon. Finally, thank you to the Monash University School of Physics and Astronomy for making me feel so welcome and ensuring that I have a wonderful experience.

References

[1] B. Allen and J.D. Romano, Phys. Rev. D **59**, 102001 (1999).
[2] E. Thrane and J.D. Romano, Phys. Rev. D **88**, (2013).
[3] J. Aasi et al. (LIGO and Virgo Collaboration) Phys. Rev. Lett. **113**, 231101 (2014).
[4] *An Introduction to LIGO and Gravitational Waves*, http://www.ligo.org/science/GW-IFO.php
[5] R.D. Branford and K.S. Thorne, *Random Processes*, (version 1206.1.K, 2012), pp.1-37.
[6] P.R. Saulson, Am. J. Phys. **65**, 501 (1997).
[7] *A Comprehensive Overview of Advanced LIGO*, https://www.advancedligo.mit.edu/summary.html
[8] A Stochastic Monitor created by Tom Callister under the supervision of Eric Thrane, https://ldas-jobs.ligo.caltech.edu/ thomas.callister/stochmonS6/stochmon.html
[9] P.R. Saulson, Class. Quantum Grav. **17** 2441, (2000).
[10] E. Thrane, N. Christensen, and R.M.S. Schofield, Phys. Rev. D **87**, 123009 (2013).
[11] E. Thrane, N. Christensen, R.M.S. Schofield, and A. Effler, Phys. Rev. D **90**, 023013 (2014).
[12] *PEM Central*, http://pem.ligo.org
[13] R.M.S. Schofield, *Results of Magnetic Coupling Investigation*, https://alog.ligo-la.caltech.edu/aLOG/index.php?callRep=11217
[14] A. Effler, *Magnetic Injections at End Stations*, https://alog.ligo-la.caltech.edu/aLOG/index.php?callRep=17851
[15] C. Wu, V. Mandic, and T. Regimbau, Phys. Rev. D **85**, 104024 (2012).
[16] V. Mandic, E. Thrane, S. Giampanis, and T. Regimbau, Phys. Rev Lett. **109**, 171102 (2012).